$MnCo_2O_4$/graphene materials derived from Mn-doped ZIF-67 and graphene nanosheets as supercapacitor electrode

WENRUI ZHANG, WEILIANG CHEN, LIANGSHUO LI, SHUHUA PANG, XIN FAN*
Guangxi Key Laboratory of Optical and Electronic Materials and Devices, College of Materials Science & Engineering, Guilin University of Technology, Guilin 541004, China

A flexible electrode of $MnCo_2O_4$/graphene (MCG) is fabricated via intercalating $MnCo_2O_4$ derived from Mn-doped ZIF-67 into graphene oxide sheets followed by hydrothermal reduction. The as-prepared materials are characterized by field emission scanning electron microscopy (FESEM) and X-Ray diffractometer. The electrochemical performances are measured by cyclic voltammetry (CV), galvanostatic charge/discharge (GCD) and electrochemical impedance spectroscopy (EIS) in a three-electrode system. Assembled asymmetric supercapacitor (ASC) is evaluated by a two-electrode method, with the active carbon and MCG as the negative electrode and positive electrode, respectively. The results show that the introduce of graphene can offer the three dimensional conductive framework. The specific capacitance of MCG electrolde can reach 1467 F/g at a current density of 1 A/g. And the GCM electrode achieves an energy density of 32.7 Wh/kg and a power density of 6250 W/kg. Furthermore, an ASC, consisting of the MCG electrode and AC electrode, retains 83.9 % capacitance retention after 9000 cycles, exhibiting good cyclic stability and durability. The high flexibility, specific capacitance and rate capacitance endow MCG to be regarded as the promising material for the high performance superconductor.

(Received January 14, 2019; accepted August 20, 2019)

Keywords: Metal-organic frameworks, Transition metal oxides, Graphene, Supercapacitor

1. Introduction

With the severe energy crisis and critical global warming derived from the excessive consumption of traditional energy resources in the past decades and the increasing energy demands nowadays, the exploration and utilization of renewable and clean energy resources such as water energy, solar energy, geothermal energy, wind energy, ocean energy, biomass energy and nuclear fusion energy etc. becomes an urgent task. Thus, the development of sustainable and efficient energy storage and conversion systems for renewable and clean energy resources seems especially important and urgent [1]. Especially, with the proliferation of microsized energy storage devices, the need for small, flexible, wearable power supplies is evidently increasing. Energy storage devices such as secondary batteries and supercapacitors (also known as electrochemical capacitors) are considered to be promising candidates [2-10]. Among them, supercapacitors have afford a very promising option for flexible energy storage applications due to long cycle life, high power density, fast charging/discharging rates, good environmental friendliness and excellent safety [11-14].

It is noted that electrode materials play a key role in the development of supercapacitors with higher capacity and long-term cycling stability in terms of the morphology, size, porosity and so forth [15,16]. Among various electrode materials, active carbons [17], natural graphite [18], carbonized cotton fabric [19] and graphene [20-22] etc. have been fabricated by depositing active materials on these substrates.

Graphene, as a new form of carbon, the intriguing two-dimensional sheet of sp^2-bonded [23], has drawn plentiful attentions owing to its exotic in-plane properties, such as extremely high electrical conductivity, flexibility, and exceptional thermal stability, large surface area and outstanding mechanical strength, which make graphene become an important active material for electrochemical energy storage [24-27]. However, the disadvantage of low capacitance and easy stack for graphene dramatically limits its more extensive applications in electrochemical capacitors [28,29]. In contrast, pseudocapacitors, including conductive polymers and transition metal oxide, based on fast and reversible redox reactions not only at the electrode surface but also at the places near the surface of the active electrode, exhibit much higher specific capacitance than carbon-based materials using electric double layer charge storage [30-32].

Transition metal oxides (TMOs) such as MO_x (M=Co, Mn, Ni, Fe, etc.) have been considered as promising electrodes due to several advantages, including their high specific/volumetric capacity, high stability and low cost [33-35]. Interestingly, mixed transition metal oxides (MTMOs), such as $NiCo_2O_4$ [36-39], $MnCo_2O_4$ [40,41], $ZnCo_2O_4$ [42,43], Ni-Mn_3O_4 [44], have drawn growing attention for electrochemical energy stroage in recent years

because of their synergistic effect and complementarity in the charge-discharge process for different valence of the transition metal ion. The coupling of two metal species could render the MTMOs with rich redox reactions which are beneficial to electrochemical applications. Besides, the various combinations of the cations and the tunable stoichiometric/non-stoichiometric compositions of the MTMOs provide vast opportunities to manipulate the electrochemical performance. On the other hand, it is well-known that the rate capability and cycle performance of electrode materials are mainly determined by the kinetics of ion diffusion and electronic conductivity [45]. Therefore, rational design of electrode materials with well-defined hierarchical porous micro/nanostructures is imperative for the further enhancement of the electrochemical properties due to their short transport pathways for electrons and ions [46].

Metal-organic frameworks (MOFs), as commonly known as coordination polymers, are a novel series of materials constructed from bridging organic linkers and metal ions. Benefiting from the ultra-high porosity, controllable pore size, crystalline nature and highly ordered structures, nanostructured MOFs have been extensively explored as precursors for preparing various nanomaterials ranging from carbon-based materials to metal-based materials with regular porous structures [47-50].

Based on these strategies, this study is focused on the improvement of the energy storage performance of graphene sheets via intercalating $MnCo_2O_4$ derived from Mn-doped ZIF-67 into graphene oxide sheets followed by hydrothermal reduction for supercapacitor electrode. It is extremely significant to integrate the benefits of the graphene and MTMOs pseudocapacitive materials, refraining from dramatic capacity fading and reduction of stability derived from their severe pulverization and agglomeration during the charge-discharge process and avoiding the stacking of graphene sheets [51]. The resultant $MnCo_2O_4$/graphene (MCG) electrode exhibits excellent property with a specific capacitance of 586.8 C/g at 1 A/g and the capacitance retention of MCG is 83.9 % even after 9000 cycles. The as-prepared MCG composite with high performance is a promising electrode material for supercapacitor.

2. Experimental

2.1. Materials and chemicals

Cobalt acetate, Manganese(II) acetate tetrahydrate were purchased from Xilong Chemical Co. Ltd. (Shantou, China). 2-Methylimidazole (2-MI), graphite were purchased from Aladdin Reagent Company (Shanghai, China). All the reagents used in the experiments were of analytical grade and used without further purification. Deionized water was used in all aqueous solution.

2.2. Fabrication of $MnCo_2O_4$/graphene composites (MCG)

$MnCo_2O_4$/graphene composites were prepared by hydrothermal method referring to our previous work [52] and the preparation process was illustrated in Fig. 1.

Typically, 6 ml graphene oxide (GO, 2 mg/mL), 8 mmol 2-MI, 2 mmol cobalt acetate, 1mmol manganese acetate, and 50 ml deionized water was placed in a stainless steel autoclave. After hydrothermal treatment, $MnCo_2O_4$/graphene precipitate (the mass ratio of $MnCo_2O_4$ to graphene in the nanocomposites is 20:1) was centrifuged and collected and freeze-dried for 48 h, and then calcined in N_2 atmosphere according to the ref. [53]. In contrast, Co_3O_4 was prepared without the presence of both manganese acetate and graphen oxide, and $MnCo_2O_4$ was prepared without the presence of graphen oxide.

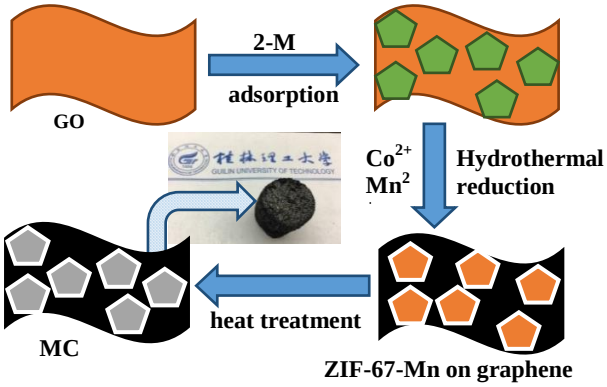

Fig. 1. Illustration of the preparation process of MCG.

2.3. Characterization

The morphology and elemental analysis were characterized by field emission scanning electron microscopy (FESEM, Hitachi-S4800). The phase of products was examined with X-Ray diffractometer (X'Pert PRO) using Cu Kα radiation (λ=0.15418 nm).

2.4. Electrochemical measurement

The work electrode was fabricated by mixing the active material (80 wt%), acetylene black (10 wt%), and polyvinylidene fluoride (10 wt%) to form a homogeneous slurry, and the blend slurry was ground vigorously using an agate mortar in DMF solution for 30 minutes, then was pressed into a nickel foam with a area of 1×1 cm^2 at 10 MPa. The electrodes was dried at 120 ℃ overnight to evaporate the solvent completely. The loading of active material on the dried electrodes was in the range of 0.2~0.6 mg/cm^3. The electrochemical performance of the Co_3O_4, $MnCo_2O_4$, MCG were measured by cyclic voltammetry (CV), galvanostatic charge/discharge (GCD) and electrochemical impedance spectroscopy (EIS) in a three-electrode system, using platinum foil and saturated

calomel electrode (SCE) as counter electrode and reference electrode, respectively, and KOH (1M) as electrolyte. Assembled asymmetric supercapacitor (ASC) was evaluated by a two-electrode method, with the mass-optimised active carbon and MCG as the negative electrode and positive electrode, respectively. CV, GCD and EIS studies were performed by a CHI 660D electrochemical workstation (Shanghai Chenhua, China), the cycle performances of all the samples mentioned were measured by a Land cell tester (CT 2001A) at a current density of 2 A/g based on mass of the active materials of the positive electrode.

The capacitance C_g (F/g) of the materials can be calculated by using the following equation:

$$C_g = \frac{\int_{V_1}^{V_2} I(V)dV}{mv(V_2 - V_1)} \quad (1)$$

$$C_g = I\Delta t/m\Delta V \quad (2)$$

V_1 (V) and V_2 (V) in equation (1) show the initial potential and end potential of CV curve, v is the scan rate (mV/s). I, Δt, m and ΔV in equation (2) represent the current (A), discharge time (s), mass loading of electrodes (g) and voltage (V) in GCD curves, respectively.

Based on the GCD curves, the specific capacity Q (C/g) of the battery-type materials was caculated as follow:

$$Q = I\Delta t \quad (3)$$

Energy density and power density are two key characteristics which determine the energy storage and charging potential of supercapacitors, and are calculated by the following equations:

$$E = 0.5CV^2/3.6 \quad (4)$$

$$P = 3600E/\Delta t \quad (5)$$

where, E (Wh/kg) is energy density, V is the voltage, P (W/kg) is power density, and Δt is the discharging time (s).

3. Results and discussion

3.1. Material characterization

The surface morphology of the prepared composites has been analyzed by FESEM.

Fig. 2(a) represents $MnCo_2O_4$ regular crystalline particles with spherical shaped sizes ca. 300~500 nm. The obtained micrographs for the $MnCo_2O_4$/graphene composites presented in Fig. 2b-c show that the surface of graphene sheets are coated with $MnCo_2O_4$ particles in globular, besides, the porous structures could be observed not only between $MnCo_2O_4$ particles and graphene sheets but also among $MnCo_2O_4$ particles. The size of $MnCo_2O_4$ grain in MCG composites becomes smaller than neat $MnCo_2O_4$ products, however, similar particles morphology for $MnCo_2O_4$ and $MnCo_2O_4$/graphene composites indicated no obvious change. Furthermore, energy dispersive X-ray spectroscopy (EDX) mapping for the chemical elements in the MCG sample was also performed and the obtained images in Fig. 2d-g confirm the presence of C, Co, Mn and O elements. Moreover, it is worth noting that the surface of graphene sheets are coated with $MnCo_2O_4$ particles throughout the selected area of study, which is consistent with Fig. 2b.

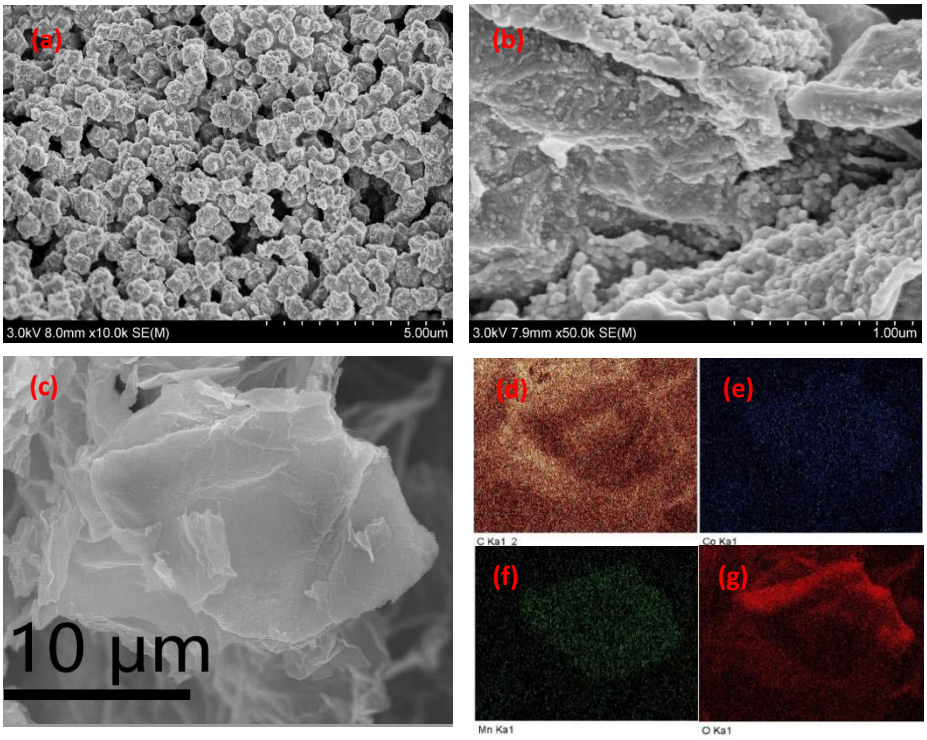

Fig. 2. SEM of (a) $MnCo_2O_4$ and (b, c) MCG sample, (d) C, (e) Co, (f) Mn and (g) O elemental distribution in MCG

To determine the crystalline structure of the MCG composites, XRD studies were employed (Fig. 3). It is obviously observed from Fig. 3 that the $MnCo_2O_4$ samples exhibited a series of diffraction peaks located at about 2θ = 18.6°, 30.6°, 36.1°, 37.9°, 44.1°, 58.3° and 64.1°, corresponding to (110), (220), (311), (222), (400), (511) and (440) crystal planes of spinel $MnCo_2O_4$ phases, respectively. All diffraction peaks matched well with the face-centered-cubic (fcc) $MnCo_2O_4$ (JCPDS no. 23-1237) with a typical spinel structure. Similar peaks are also observed in the diffraction pattern of the MCG composites, but peak intensities appear relatively low except (311) crystal plane. Additionally, there are no impurity diffraction peaks, indicating the precursor completely transforms to $MnCo_2O_4$.

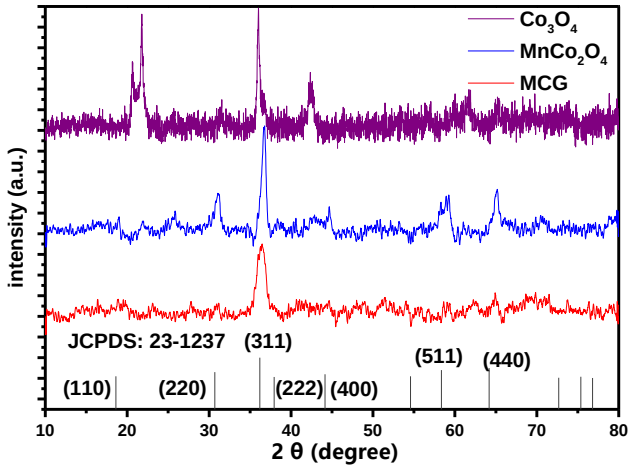

Fig. 3. XRD patterns of Co_3O_4, $MnCo_2O_4$, MCG samples

3.2. Electrochemical characterization

CV is used to evaluate the electrochemical performance of the fabricated supercapacitor electrodes. CV characteristics of Co_3O_4, $MnCo_2O_4$ and MCG composite within a potential window of 0-0.5 V at a scan rate of 5 mV/s are provided in Fig. 4a.

As shown in Fig. 4a, obvious redox peaks observed in all CV curves of Co_3O_4, $MnCo_2O_4$, MCG samples suggested a pseudocapacitive electrochemical behaviour, the typical redox peaks observed in CV curves of Co_3O_4 and $MnCo_2O_4$ material were originated from the reversible transition between the oxidation states of cobalt (Co^{3+}/Co^{4+}) and manganese ions ($Mn^{2+}/Mn^{3+}/Mn^{4+}$) [54,55]. On the other hand, MCG composite exhibits a nearly rectangular shape with obvious peaks for oxidation and reduction, indicating both a characteristic of the electric double-layer capacitance behaviour of carbon-based materials and a pseudocapacitive electrochemical behaviour of transition metal oxide. Moreover, MCG composite shows the highest current density among all the electrodes, implying its best capacitive performance. During the charge-discharge process, the fast redox reactions occurring in the surface of the electrodes may be described as follows [56]:

$$MnCo_2O_4 + H_2O + OH^- \leftrightarrow 2CoOOH + MnOOH^+ e^-$$
$$CoOOH + OH^- \leftrightarrow CoO_2 + H_2O + e^-$$
$$MnOOH + OH^- \leftrightarrow MnO_2 + H_2O + e^-$$

Interestingly, MCG could be charged to 0.5 V more than 0.45 V of Co_3O_4 or $MnCo_2O_4$, which efficiently promoted the energy density of the materials by enhance the V according to the equation (3). The CV curves of the MCG electrode at the scan rates of 5, 10, 20, 50 and 100 mV/s are presented in Fig. 4b, and the values of C_g calculated according to the equation (1) were 1221.5, 1116.6, 1024.4, 986.7 and 846.5 F/g, respectively. From the curves, it can be observed that the anodic peaks shift towards right and the cathodic peaks shift towards left as well as the current density gradually with the increasing scan rates, showing that the electrochemical process is diffusion-controlled [57]. It is worth noting that, MCG still maintained a specific capacitance as high as 846.5 F/g at 100 mV/s, while the specific capacitances of Co_3O_4 and $MnCo_2O_4$ decreased rapidly to 390.9 and 453.6 F/g at the same scan rate, respectively, the capacitance of MCG hybrid material was ~2 times higher than that of Co_3O_4 or $MnCo_2O_4$. Even though at scan rate of 5 mV/s, the specific capacitances of Co_3O_4 and $MnCo_2O_4$ were only 657 and 724.9 F/g, which is less than 846.5 F/g at 100 mV/s for MCG. The specific capacitance varying with scan rate for Co_3O_4, $MnCo_2O_4$ and MCG, which were calculated from equation (1), were shown in Fig. 4c. These results illustrated the high capacity at a wide range of scan rates, and excellent rate capability of MCG composite.

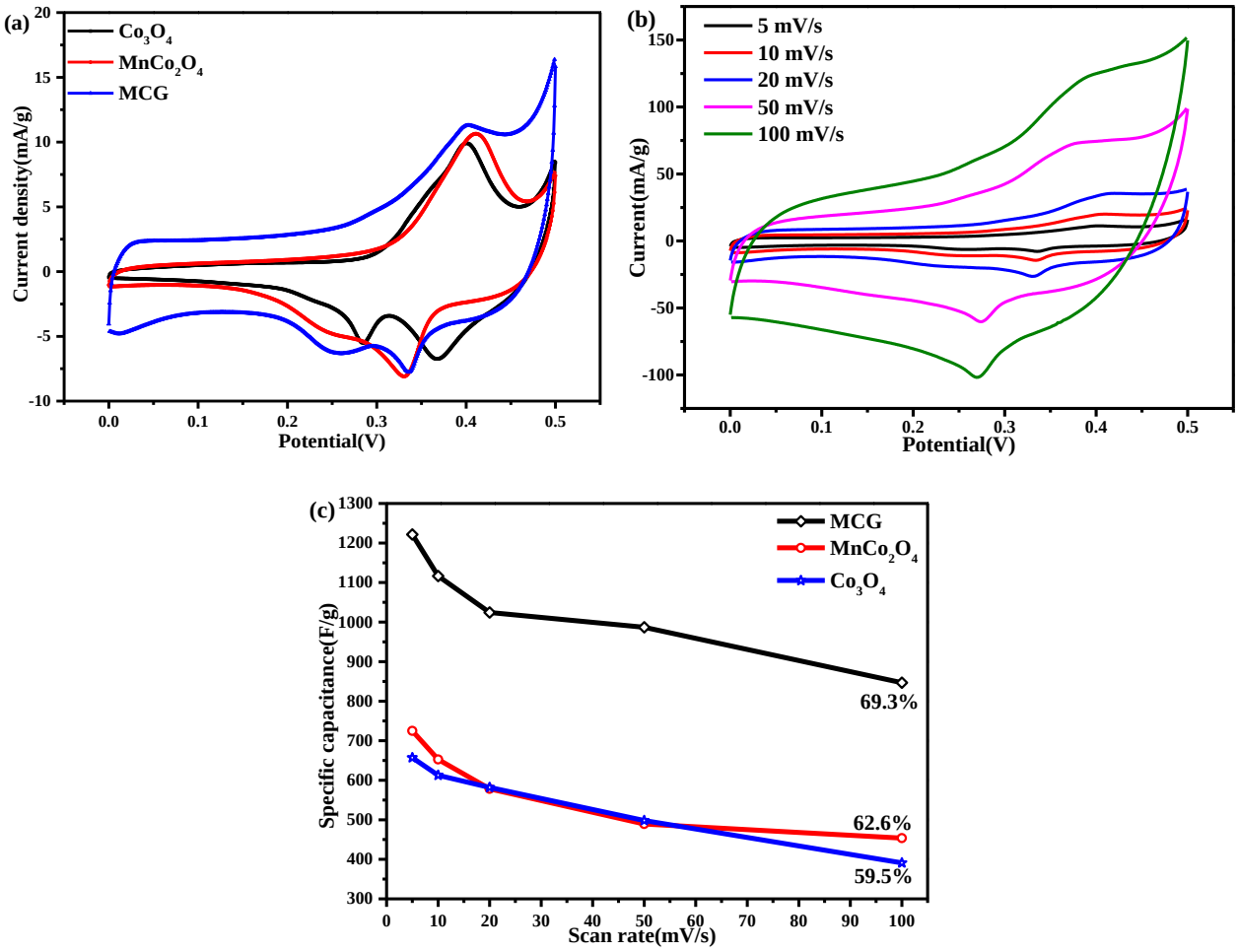

Fig. 4. (a) CV curves at 5mV/s of Co_3O_4, $MnCo_2O_4$ and MCG samples and (b) CV curves of MCG samples at 5-100 mV/s, and (c) Variations of the specific capacitance with scan rate for Co_3O_4, $MnCo_2O_4$ and MCG

GCD provides a method to measure the total resistance and practically achievable capacitances of the electrodes. As can be seen in Fig. 5a, the discharge time of MCG is ~3 times that of $MnCo_2O_4$ or Co_3O_4, indicating the capacitance performance enhancement of MCG. Fig. 5b presents the GCD curves of the MCG electrode at current densities of 1, 2, 5, 10 and 20 A/g, and the corresponding values of C_g are 1467.1, 1262.6, 1122.5, 1037.5 and 943.1 F/g, respectively, the corresponding values of Q are 586.8, 505.0, 449.0, 415.0, 377.24 C/g. GCD curves of MCG at different current densities exhibited a non-linear triangular shaped charge/discharge curve, implying that its capacitance is attributed to both pure electric double layer (triangular shape) and faradic reactions (non-linear shape). Besides, all charge/discharge curves still exhibited a similar shape with the increase of current density, revealing the ideal capacitive behaviours of MCG composite. The specific capacitance varying with current density for Co_3O_4, $MnCo_2O_4$ and MCG, which were calculated from equation (2), were shown in Fig. 5c. These results were in accordance with the results originated from Fig. 4c.

The specific capacitances of various composites applied in supercapacitor electrodes were displayed in Table 1. It can be seen from the different specific capacitance that the electrochemical performance of MCG is superior to most recently reported metal oxide/graphene composite materials.

The Ragone plots of Co_3O_4, $MnCo_2O_4$, MCG electrodes derived from the charge/discharge curves were shown in Fig. 5d. Remarkably for MCG, the energy density was higher than that for Co_3O_4 or $MnCo_2O_4$, especially, an energy density of 50.9 Wh/kg can be obtained at a power density of 312.5 W/kg and the energy density still retains 32.7 Wh/kg even at high power density of 6250 W/kg. So these kinds of MCG electrode materials have great potential for supercapacitors.

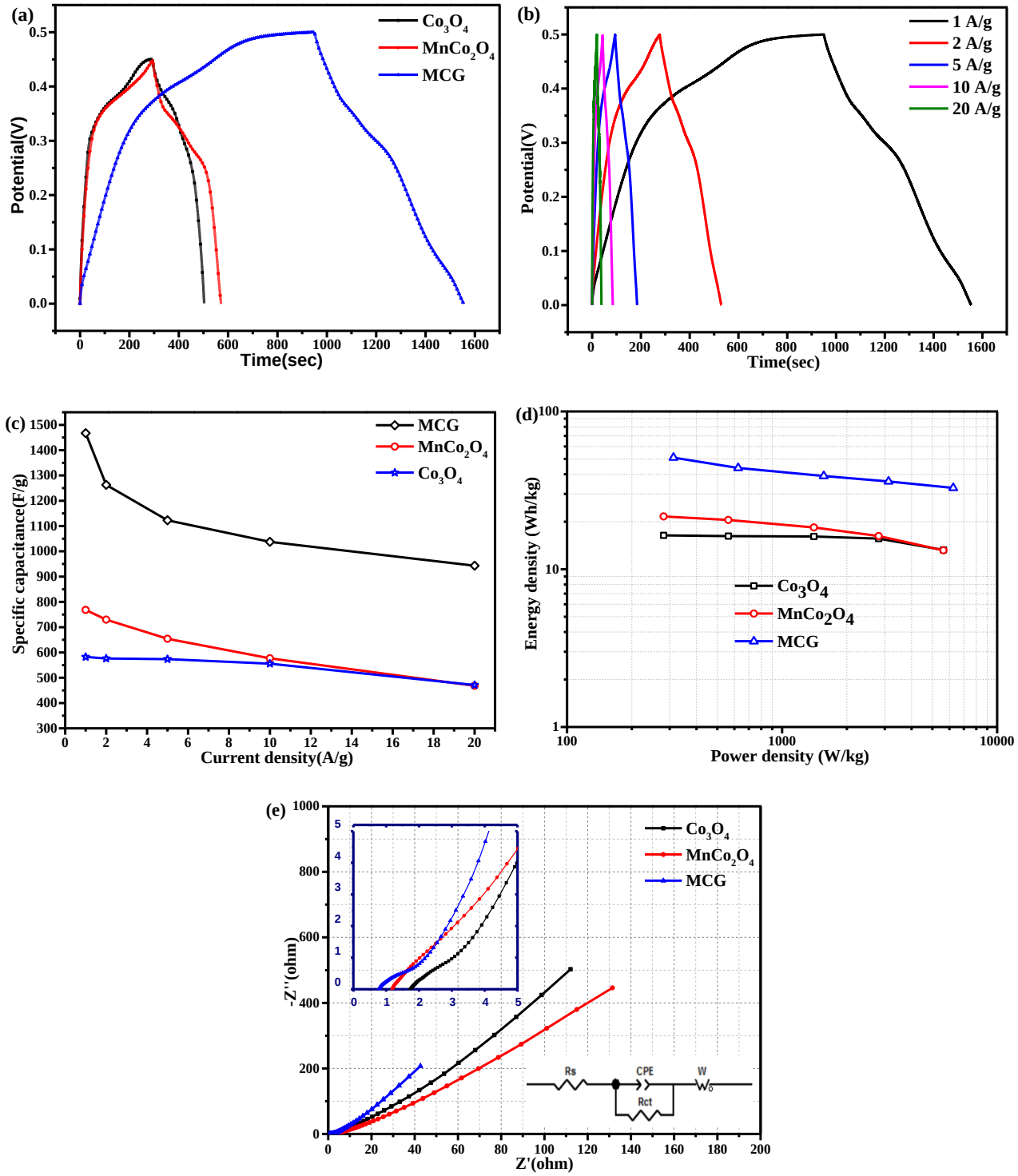

*Fig. 5. (a) GCD curves of Co_3O_4, $MnCo_2O_4$ and MCG at 1 A/g, (**b**) GCD curves of MCG at various current densities, (**c**) Variations of the specific capacitance with current density for Co_3O_4, $MnCo_2O_4$ and MCG, (**d**) Regone plot and (**e**) EIS curves of Co_3O_4, $MnCo_2O_4$ and MCG samples*

In Fig. 5e, EIS curve showed a semicircle at higher frequency and a sloped line at lower frequency, which relate to the charge transfer resistance and diffusion resistance, respectively. The point where the semicircle at the high frequency intercepts the x-axis (left inset of Fig. 5e) can be used to determine the equivalent series resistance (ESR) (right inset of Fig. 5e), corresponding to the electrode material/electrolyte interface resistance. The ESR values of Co_3O_4, $MnCo_2O_4$, MCG were 1.75, 1.09, 0.58 Ω, respectively, which suggests that MCG sample possesses higher electrical conductivity due to the addition of graphene. At low frequency range, the MCG electrode also

has a more ideal vertical line than Co_3O_4 or $MnCo_2O_4$, which demonstrates that the MCG electrode has reduced the charge transfer resistance (R_{ct}) and enhanced the ion diffusion of electrolyte. This is mainly due to the two facts (observed in Fig. 2b): (1) porous structures not only between $MnCo_2O_4$ particles and graphene sheets but also among $MnCo_2O_4$ particles, which is beneficial for the access of electrolyte into the electrode material, 61 and (2) the contact between $MnCo_2O_4$ particles and graphene sheets, which is important for the transport of electrolyte ions into the underneath part of the composite to achieve outstanding electrochemical performance [63,64].

Table 1. Comparison of electrochemical performance of metal oxides based materials

Electrode material	Specific capacitance (F/g)	Retention of capacitance	Ref.
MCG	1467 (1 A/g) 543 (20 A/g)	83.9 % after 9000 cycles	This work
Co_3O_4	1095(1 A/g)	71 % after 2000 cycles	[58]
MnO_2	342(0.5 A/g)	90 % after 2000 cycles	[59]
MnOOH	1120 (1 A/g)	97 % after 1000 cycles	[60]
Co_3O_4/ Graphene	443 (5 A/g)	97 % after 1000 cycles	[61]
MnO_2/ Graphene	278.5 (1 A/g)	93.5 % after 10000 cycles	[62]
$MnCo_2O_4$ nano cages	1763 (1 A/g) 840 (10 A/g)	95 % after 4500 cycles	[41]
Mesoporous $MnCo_2O_4$	1487 (1 A/g)	93.3 % after 2000 cycles	[42]

3.3. Asymmetric supercapacitor based on MCG and active carbon (AC)

The electrochemical performance of ASCs based on MCG and active carbon were evaluated using CV and GCD methods. The positive electrode of the ASCs (MCG//AC) is MCG with a globular morphology that provides convenient paths to a great number of ions to permeate deep into the internal framework of MCG, which improves optimization utilization of electrode materials. On the other hand, the nanostructure framework of MCD and the porous struture of active carbon play an important role by providing fast charge transfer through their connected pore structure. Therefore, this well-designed ASCs will combine the advantages of the two materials to obtain high energy density and power density. As can be seen from Fig. 6a, the CV curves are similar rectangular and symmetric in shape, even though the potential window is extended up to 1.6 V (Fig. 6a and 6b), illustrating a combination of both electric double-layer and pseudocapacitive types of capacitance as well as ideal capacitive performance with excellent reversibility. Fig. 6b reveals the GCD profiles at different current densities. The discharge curves are almost symmetrical to the corresponding charge curves, suggesting excellent charge-storage reversibility of the ASC. Nyquyst plot of ASC was shown in Fig. 6c, the ESR of the devices is 0.87 Ω, which could be seen from the value the plot intercepts with the x-axis. In Fig. 6d, remarkably, the capacitance retention of MCG is 83.9 % even after 9000 cycles. Interestingly, ASC shows better cycle life than MCG alone, it is due to the fact that MCG and AC contributed to the performance together.

To demonstrate the practical usage of the ASCs, the ASCs were fabricated into coin cells to power the light-emitting-diode (LED) (the inset in Fig. 6c). After fully charged, 2 cells of the ASC(MCG//AC) could light up a red LED indicator (rated voltage 2.1V) for more than 70 seconds, suggesting the promising practical application of the ASC(MCG//AC) in the energy-storage fields.

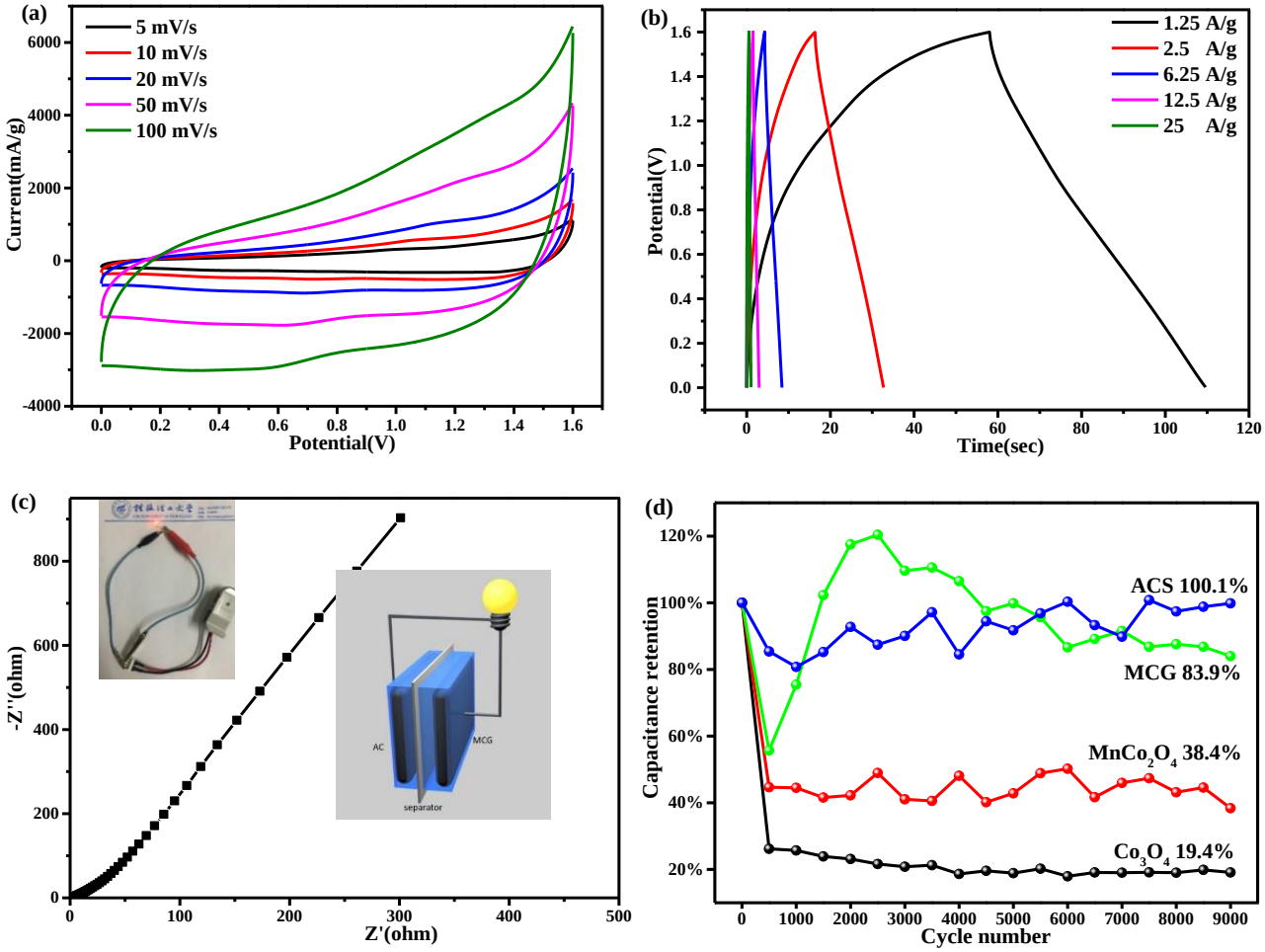

Fig. 6. (a) CV, (b) GCD, (c) EIS of ASC, (d) cycle stability of Co_3O_4, $MnCo_2O_4$, MCG and ASC

4. Conclusions

In summary, MCG composites with high performance are successfully prepared via intercalating $MnCo_2O_4$ derived from Mn-doped ZIF-67 into graphene oxide sheets followed by hydrothermal reduction for supercapacitor electrode. The results demonstrate that the nanostructure framework of granular metal oxides is coated on the surface of graphene nanosheets, resulting in greatly shorting the migration and diffusion paths of electrolyte ions during the rapid charge/discharge process. The specific capacitance of GCM electrode can reach 586.8 C/g at 1 A/g. The GCM electrode achieves an energy density of 32.7 Wh/kg and a power density of 6250 W/kg. Furthermore, an ASC which consists of the MCG electrode and AC electrode retains 83.9 % capacitance retention after 9000 cycles, exhibiting good cyclic stability and durability. All these characterization and electrochemical measurement results indicate the MCG is a promising electrode and can be applied in the flexible energy storage devices.

Acknowledgments

This research was funded by Innovation Project of Guangxi Graduate Education (YCSW2018153, JGY2018073), and Open Funds of Key Laboratory of New Processing Technology for Nonferrous Metal and Materials of Ministry of Education (14KF-1, 19AA-18).

References

[1] P. Simon, Y. Gogotsi, Nature Mater. **7**, 845 (2008).
[2] Q. Chen, T. Zhang, X. Qiao, D. Li, J. Yang, J. Power Sources **234**, 197 (2013).
[3] Q. Chen, Y. Wang, T. Zhang, W. Yin, J. Yang, X. Wang, Electrochim. Acta **83**, 65 (2012).
[4] Y. Li, G. Pan, W. Xu, J. Yao, L. Zhang, J. Power Sources **307**, 114 (2016).
[5] Y. Li, Y. Zheng, J. Yao, J. Xiao, J. Yang, S. Xiao, RSC Adv. **7**, 31287 (2017).
[6] Y. He, J. Zhang, Q. Li, Y. Hao, J. Yang, L. Zhang, C. Wang, J. Alloys Comp. **715**, 304 (2017).
[7] J. Yao, Y. Li, Y. Li, Y. Zhu, H. Wang, J. Power Sources **224**, 236 (2013).
[8] Y. Li, J. Yao, Y. Zhu, Z. Zou, H. Wang, J. Power Sources **203**, 177 (2012).
[9] N. Wang, Q. Liu, D. Kang, J. Gu, W. Zhang, D. Zhang, ACS Appl. Mater. Interfaces **8**, 16035 (2016).
[10] J. O. Thostenson, Z. Li, C. H. J. Kim, A. Ajnsztajn,

C. B. Parker, J. Liu, A. V. Peterchev, J. T. Glass, S. M. Goetz, J. Electrochem. Soc. **165**, B3122 (2018).
[11] A. Tang, D. He, Z. He, G Xu, H. Song, R. Peng, J. Power Sources **275**, 888 (2015).
[12] G. R. Xu, J. J. Shi, W. H. Dong, Y. Wen, X. P. Min, A. P. Tang, J. Alloy. Compd. **630**, 266 (2015).
[13] F. Zhou, Q. Liu, J. Gu, W. Zhang, D. Zhang, Electrochim. Acta **170**, 328 (2015).
[14] R. Naz, M. Imtiaz, Q. Liu, L. Yao, J. Gu, Carbon **152**, 697 (2019).
[15] S. Wang, Z. Kang, S. Li, J. Tu, J. Zhu, S. Jiao, J. Electrochem. Soc. **164**, A3319 (2017).
[16] H. Chen, C. Huang, J. Jiang, J. Electrochem. Soc. **165**, A448 (2018).
[17] G. Chaudhary, A. K. Sharma, P. Bhardwaj, K. Kant, I. Kaushal, A. K. Mishra, J. Energy Chem. **26**, 175 (2017).
[18] R. Yuksel, N. Uysal, A. Aydinli, H. E. Unalan, J. Electrochem. Soc. **165**, A283 (2018).
[19] D. S. Su, G. Centi, J. Energy Chem. **22**, 151 (2013).
[20] L. Bao, X. Li, Adv. Mater. **24**, 3246 (2012).
[21] Z. Xiong, C. Liao, W. Han, X. Wang, Adv. Mater. **27**, 4469 (2015).
[22] Y. Hu, H. H. Cheng, F. Zhao, N. Chen, L. Jiang, Z. H. Feng, L. T. Qu, Nanoscale **6**, 6448 (2014).
[23] Z. Niu, L. Zhang, L. Liu, B. Zhu, H. Dong, X. Chen, Adv. Mater. **25**, 4035 (2013).
[24] Y. Zheng, W. Pann, D. Zhengn, C. Sun, J. lectrochem. Soc. **163**, D230 (2016).
[25] Y. Wang, D. Zhou, D. Zhao, M. Hou, C. Wang, Y. Xia, J. Electrochem. Soc. **160**, A98 (2013).
[26] M. J. Allen, V. C. Tung, R. B. Kaner, Chem. Rev. **110**, 132 (2010).
[27] G. Wang, L. Zhang, J. Zhang, Chem. Soc. Rev. **41**, 797 (2012).
[28] A. Manta, M. Gresil, C. Soutis, App. Compos. Mater. **24**, 281 (2017).
[29] S. Yang, K. Chang, H. Tien, Y. Lee, S. Li, Y. Wang, J. Wang, C. Ma, C. Hu, J. Mater. Chem. **21**, 2374 (2011).
[30] H. Yavuz, J. Bai, App. Compos. Mater. **25**, 661 (2018).
[31] B. Ou, R. Huang, W. Wang, H. Zhou, C. He, RSC Adv. **4**, 43212 (2014).
[32] D. W. Wang, F. Li, H. M. Cheng, J. Power Sources **185**, 1563 (2008).
[33] H. Jiang C. Z. Li, T. Sun, J. Ma, Nanoscale **4**, 807 (2012).
[34] P. Poizot, S. Laruelle, S. Grugeon, L. Dupont, J. M. Tarascon, Nature **407**, 496 (2000).
[35] G. R. Xu, X. P. Min, Q. L. Chen, Y. Wen, A. P. Tang, H. S. Song, J. Alloy. Compd. **691**, 1018 (2017).
[36] G. R. Xu, Y. Wen, X. P. Min, W. H. Dong, A. P. Tang, H. S. Song, Electrochim. Acta **186**, 133 (2015).
[37] H. Jiang, J. Ma, C. Li, Chem. Commun. **48**, 4465 (2012).
[38] G. Zhang, X. W. Lou, Adv. Mater. **25**, 976 (2013).
[39] G. Gao, H. B. Wu, B. Dong, S. Ding, X. W. Lou, Adv. Sci. **2**, 1400014 (2015).
[40] Y. H. He, X. Xiao, L. Gao, S. H. Li, Y. Shen, Chemelectrochem **4**, 607 (2017).
[41] Y. Dong, Y. Wang, Y. Xu, C. Chen, Y. Wang, L. Jiao, H. Yuan, Electrochim. Acta **225**, 39 (2017).
[42] A. K. Mondal, D. Su, S. Chen, A. Ung, H. S. Kim, G. Wang, Chemistry **21**, 1526 (2015).
[43] S. Wang, J. Pu, Y. Tong, Y. Cheng, Y. Gao, Z. Wang, J. Mater. Chem. A **2**, 5434 (2014).
[44] B. Guan, D. Guo, L. Hu, G. Zhang, T. Fu, W. Ren, J. Li, Q. Li, J. Mater. Chem. A **2**, 16116 (2014).
[45] Y. Hou, Y. W. Cheng, T. Hobson, J. Liu, Nano Lett. **10**, 2727 (2010).
[46] H. Jiang, T. Zhao, J. Ma, C. Y. Yan, C. Z. Li, Chem. Commun. **47**, 1264 (2011).
[47] B. Zheng, H. Wang, Z. Wang, N. Ozaki, C. Hang, X. Luo, L. Huang, W. Zeng, M. Yang, J. Duan, Chem. Commun. **52**, 12988 (2016).
[48] B. Li, H. M. Wen, Y. Zhou, G. Qian, B. Chen, Adv. Mater. **28**, 8819 (2016).
[49] Y. V. Kaneti, J. Tang, R. R. Salunkhe, X. Jiang, A. Yu, K. C. Wu, Y. Yamauchi, Adv. Mater. **29**, 1604898 (2017).
[50] B. Y. Guan, A. Kushima, L. Yu, S. Li, J. Li, X. W. Lou, Adv. Mater. **29**, 1605902 (2017).
[51] G. Yu, L. Hu, N. Liu, H. Wang, M. Vosgueritchian, Y. Yang, Y. Cui, Z. Bao, Nano Lett. **11**, 4438 (2011).
[52] X. Fan, W. Chen, S. Pang, W. Lu, Y. Zhao, Z. Liu, D. Fang, Chem. Phys. Lett. **689**, 162 (2017).
[53] R. R. Salunkh,, J. Tang, Y. Kamachi, T. Nakato, J. H. Kim, Y. Yamauchi, ACS Nano **9**, 6288 (2015).
[54] S. Sahoo, K. K. Naik, C. S. Rout, Nanotechnology **26**, 455401 (2015).
[55] Y. N. Xu, X. F. Wang, C. H. An, Y. J. Wang, J. F. Jiao, H. T. Yuan, J. Mater. Chem. A **2**, 16480 (2014).
[56] W. F. Wei, X. W. Cui, W. X. Chen, D. G. Ivey, Chem. Soc. Rev. **40**, 1697 (2011).
[57] H. W. Park, T. Kim, J. Huh, M. Kang, J. E. Lee, H. Yoon, ACS Nano **6**, 7624 (2012).
[58] Y. You, M. Zheng, L. Ma, X. Yuan, B. Zhang, Q. Li, F. Wang, J. Song, D. Jiang, P. Liu, L. Ma, W. Shen, Nanotechnology **28**, 105604 (2017).
[59] R. S. Kalubarme, H. S. Jadhav, C. J. Park, Electrochim. Acta **87**, 457 (2013).
[60] A. A. Lobinsky, V. P. Tolstoy, J. Energy. Chem. **26**, 336 (2017).
[61] S. Huang, Y. Jin, M. Jia, Electrochim. Acta **95**, 139 (2013).
[62] J. Zhong, F. Yi, A. Gao, D. Shu, Y. Huang, Z. Li, W. Zhu, C. He, T. Meng, S. Zhao, Chemelectrochem **4**, 1088 (2017).
[63] I. Shakir, Electrochim. Acta **132**, 490 (2014).
[64] J. Yao, Y. Li, R. C. Massé, E. Uchaker, G. Cao, Energy Storage Mater. **11**, 205 (2018).

*Corresponding author: xfan@glut.edu.cn